Published by Institute of Physics Publishing for SISSA
Received: *July 20, 2005*
Accepted: *August 3, 2005*
Published: *September 12, 2005*

Dark matter and $B_s \to \mu^+ \mu^-$ with minimal SO_{10} soft SUSY breaking II

Radovan Dermíšek,[a] **Stuart Raby,**[b] **Leszek Roszkowski**[c] **and Roberto Ruiz de Austri**[d]

[a]*Davis Institute for High Energy Physics, University of California, Davis, CA 95616, U.S.A.*
[b]*Department of Physics, The Ohio State University, 174 W. 18th Ave., Columbus, Ohio 43210, U.S.A.*
[c]*Department of Physics and Astronomy, University of Sheffield, Sheffield S3 7RH, U.K.*
[d]*Departamento de Física Teórica C-XI and Instituto de Física Teórica C-XVI Universidad Autónoma de Madrid, Cantoblanco, 28049 Madrid, Spain*
E-mail: dermisek@physics.ucdavis.edu, raby@pacific.mps.ohio-state.edu, L.Roszkowski@sheffield.ac.uk, rruiz@delta.ft.uam.es

Abstract: We update and extend to larger masses our previous analysis of the MSSM with minimal SO_{10} [$\mathrm{MSO}_{10}SM$] soft SUSY breaking boundary conditions. We find a well-defined, narrow region of parameter space which provides the observed relic density of dark matter, in a domain selected to fit precision electroweak data, including top, bottom and tau masses. The model is highly constrained which allows us to make several predictions. We find the light Higgs mass $m_h \leq 121 \pm 3\,\mathrm{GeV}$ and also upper bounds on the mass of the gluino $m_{\tilde{g}} \lesssim 3.1\,\mathrm{TeV}$ and lightest neutralino $m_\chi \lesssim 450\,\mathrm{GeV}$. As the CP odd Higgs mass m_A increases, the region of parameter space consistent with WMAP data is forced to larger values of $M_{1/2}$ and smaller values of m_h. Hence, we find an upper bound $m_A \lesssim 1.3$ TeV. This in turn leads to lower bounds on $\mathrm{BR}(B_s \to \mu^+ \mu^-) > 10^{-8}$ (assuming minimal flavor violation) and on the dark matter spin independent detection cross section $\sigma_p^{SI} > 10^{-9}$ pb. Finally, we extend our previous analysis to include WIMP signals in indirect detection and find prospects for WIMP detection generally much less promising than in direct WIMP searches.

Keywords: Supersymmetry Phenomenology, Beyond Standard Model.

JHEP09(2005)029

Contents

1. Introduction

The constrained minimal supersymmetric standard model [CMSSM] [1] is a well defined model for soft SUSY breaking with five independent parameters given by $m_0,\ M_{1/2},\ A_0,$ $\tan\beta$ and $sign(\mu)$. It has been used extensively for benchmark points for collider searches, as well as for astrophysical and dark matter analyses. The economy of parameters in this scheme makes it a useful tool for exploring SUSY phenomena. However the CMSSM misses regions of soft SUSY breaking parameter space which give qualitatively different predictions. In a previous paper [2] we considered an alternate scheme, the minimal SO_{10} supersymmetric model [$\mathrm{MSO}_{10}\mathrm{SM}$] [3], which is well motivated and opens up a qualitatively new region of parameter space. In light of the recent WMAP analysis and recent improved limits from DZero and CDF on the branching ratio $\mathrm{BR}(B_s \to \mu^+\,\mu^-)$, and from CDMS on the dark matter direct detection cross section, we have decided to reanalyze the $\mathrm{MSO}_{10}\mathrm{SM}$, including updated data and extending the region of parameter space to larger values of $m_{16} \geq 3\,\mathrm{TeV}$ and $m_A \geq 500\,\mathrm{GeV}$.

The recent WMAP data [4] provides an important constraint on the model. The dark matter candidate in this model is the lightest neutralino. However, since the scalar masses of the first two families are of order $m_{16} > 1.2\,\mathrm{TeV}$, and the third generation sfermions (except for the stops) also tend to be heavy, the usually dominant annihilation channels, for the neutralino LSP to light fermions via t-channel sfermion exchange, are suppressed. On the other hand, the process $\chi\chi \to f\bar{f}$ via s-channel CP odd Higgs A exchange becomes important. This is due to the enhanced A coupling to down-type fermions, which is proportional to $\tan\beta$, and because, in contrast to heavy scalar exchange, the process is not p-wave suppressed.

We also compute the branching ratio for the process $B_s \to \mu^+ \mu^-$ due to A exchange [5, 6]. It is absolutely essential to include this latter constraint in our analysis, particularly in light of the published DZero bound $\mathrm{BR}(B_s \to \mu^+ \mu^-) < 5.0 \times 10^{-7} (4.1 \times 10^{-7})$ at 95% (90%) CL [7] and the new preliminary CDF bound $< 2.0 \times 10^{-7}$ at 95% CL [8] and DZero bound $< 3.7 \times 10^{-7}$ at 95% CL [9].

The CDMS Collaboration has recently improved the upper limit on the spin independent dark matter WIMP elastic scattering cross section on a proton, σ_p^{SI}, down to 2×10^{-7} pb (at low WIMP mass) [10]. A further improvement by an order of magnitude is foreseen within a year. We update our previous results for σ_p^{SI} and show that a large fraction of the parameter space will be probed with currently running detectors, and will be completely explored with a new round of "one-tonne" detectors which plan to reach down to $\sigma_p^{SI} \gtrsim 10^{-10}$ pb.

In addition, we now evaluate prospects for indirect detection of WIMPs in muon flux from WIMP annihilation in the Sun, a gamma ray flux from the Galactic center, as well as antiproton and positron fluxes from the Galactic halo. Here detection prospects are somewhat varied and, especially in the case of the gamma ray flux, strongly depend on an adopted model of the Galactic halo.

The paper is organized as follows. In section 2 we review the $\mathrm{MSO_{10}SM}$, describe its virtues and outline the analysis. Then in section 3 for different values of m_{16} and m_A we compute $\mathrm{BR}(B_s \to \mu^+ \mu^-)$, the cosmological dark matter density $\Omega_\chi h^2$, etc. The major results of the paper are found in section 3.1. We discuss the upper bound on the CP odd Higgs mass, m_A, and the resulting lower bound on $\mathrm{BR}(B_s \to \mu^+ \mu^-)$. CDF and DZero can potentially probe the entire allowed range. We also consider the predictions for underground dark matter searches. The entire expected range can be fully explored at the next level of underground dark matter searches. We also consider indirect dark matter searches. Finally in table 1 we give Higgs and SUSY spectra relevant for collider searches for four representative points in SUSY parameter space. We summarize our results in section 4.

2. Minimal $\mathrm{SO_{10}}$ SUSY model — $\mathrm{MSO_{10}SM}$

2.1 Framework

Since there are several distinct theories in the literature called the minimal SO(10) SUSY model, let us briefly describe here the properties of our minimal SO_{10} SUSY model [$\mathrm{MSO_{10}SM}$] [3]. Quarks and leptons of one family reside in the **16** dimensional representation, while the two Higgs doublets of the MSSM reside in one **10** dimensional representation. For the third generation we assume the minimal Yukawa coupling term given by λ **16 10 16**. On the other hand, for the first two generations and for their mixing with the third, we assume a hierarchical mass matrix structure due to effective higher dimensional operators. Hence the third generation Yukawa couplings satisfy $\lambda_t = \lambda_b = \lambda_\tau = \lambda_{\nu_\tau} = \lambda$.

Soft SUSY breaking parameters are also consistent with SO_{10} with (1) a universal gaugino mass $M_{1/2}$, (2) a universal squark and slepton mass m_{16},[1] (3) a universal scalar

Higgs mass m_{10}, and (4) a universal A parameter A_0. In addition we have the supersymmetric (soft SUSY breaking) Higgs mass parameters μ ($B\mu$). $B\mu$ may, as in the CMSSM, be exchanged for $\tan\beta$. Note, not all of these parameters are independent. Indeed, in order to fit the low energy electroweak data, including the third generation fermion masses, it has been shown that A_0, m_{10}, m_{16} must satisfy the constraints [3]

$$A_0 \approx -2\, m_{16}\,; \qquad m_{10} \approx \sqrt{2}\, m_{16} \tag{2.1}$$

$$m_{16} > 1.2\,\text{TeV}\,; \qquad \mu,\ M_{1/2} \ll m_{16} \tag{2.2}$$

with

$$\tan\beta \approx 50\,. \tag{2.3}$$

This result has been confirmed by several independent analyses [11, 12].[2] Although the conditions (eqs. 2.1, 2.2) are not obvious, it is however easy to see that (eq. (2.3)) is simply a consequence of third generation Yukawa unification, since $m_t(m_t)/m_b(m_t) \sim \tan\beta$.

One loop threshold corrections at the GUT scale lead to two significant parameters we treat as free parameters, although they are calculable in any GUT. The first is a correction to gauge coupling unification given by

$$\epsilon_3 \equiv \frac{[\alpha_3(M_G) - \tilde{\alpha}_G]}{\tilde{\alpha}_G} \tag{2.4}$$

where the GUT scale M_G is defined as the scale where $\alpha_1(M_G) = \alpha_2(M_G) \equiv \tilde{\alpha}_G$. The second is a Higgs splitting mass parameter defined by

$$\Delta m_H^2 \equiv \frac{(m_{H_d}^2 - m_{H_u}^2)}{2 m_{10}^2}\,. \tag{2.5}$$

In order to fit the low energy data we find $\epsilon_3 \approx -4\%$ and $\Delta m_H^2 \approx 13\%$ [3]. The largest corrections to ϵ_3 come from the Higgs and SO_{10} breaking sectors, while the correction to Δm_H^2 is predominantly due to the right-handed τ neutrino. Note, for $M_{\bar{\nu}_\tau} \sim 5.8\times 10^{13}$ GeV, the necessary Higgs splitting is reduced to 7% [14].

Finally, as a bonus, these same values of soft SUSY breaking parameters, with $m_{16} \gg$ TeV, result in two very interesting consequences. Firstly, it "naturally" produces an inverted scalar mass hierarchy [ISMH] [15]. With an ISMH squarks and sleptons of the first two generations obtain mass of order m_{16} at M_Z. The stop, sbottom, and stau, on the other hand, have mass less than (or of order) a TeV. An ISMH has two virtues. (1) It preserves "naturalness" (for values of m_{16} which are not too large), since only the third generation squarks and sleptons couple strongly to the Higgs. (2) It ameliorates the SUSY CP and flavor problems, since these constraints on CP violating angles or flavor violating squark and slepton masses are strongest for the first two generations, yet they are suppressed as $1/m_{16}^2$. For $m_{16} >$ a few TeV, these constraints are weakened [16 – 18].

[1] SO_{10} does not require all sfermions to have the same mass. This however may be enforced by non-abelian family symmetries or possibly by the SUSY breaking mechanism.

[2] Note, different regions of parameter space consistent with Yukawa unification have also been discussed in [11 – 13].

Secondly, Super-Kamiokande bounds on $\tau(p \to K^+\bar{\nu}) \; > 2.3 \times 10^{33}$ yrs [19] constrain the contribution of dimension 5 baryon and lepton number violating operators. These are however minimized with $\mu,\; M_{1/2} \ll m_{16}$ [20].

2.2 Phenomenological analysis

We use a top-down approach with a global χ^2 analysis [21]. The input parameters are defined by boundary conditions at the GUT scale. The 11 input parameters at M_G are given by: three gauge parameters M_G, $\alpha_G(M_G)$, ϵ_3; the Yukawa coupling λ, and 7 parameters, including μ, and the 6 soft SUSY breaking parameters $M_{1/2}$, A_0, $\tan\beta$ (replacing $B\mu$), m_{16}^2, m_{10}^2, Δm_H^2. These are fit in a global χ^2 analysis defined in terms of physical low energy observables. Note we keep three parameters (m_{16}, μ, $M_{1/2}$) fixed; while minimizing χ^2 with the remaining 8 parameters. Below we plot χ^2 contours as a function of $\mu,\; M_{1/2}$ for different values of m_{16}. We use two (one) loop renormalization group [RG] running for dimensionless (dimensionful) parameters from M_G to M_Z.[3] We require electroweak symmetry breaking using an improved Higgs potential, including m_t^4 and m_b^4 corrections in an effective 2-Higgs doublet model below $M_{\rm SUSY} = \sqrt{\frac{1}{2}(m_{\tilde{t}_1}^2 + m_{\tilde{t}_2}^2)}$ [22, 23].

The χ^2 function includes 9 observables; 6 precision electroweak data α_{EM}, G_μ, $\alpha_s(M_Z)$, M_Z, M_W, $\rho_{\rm NEW}$ and the 3 fermion masses $M_{\rm top}$, $m_b(m_b)$, M_τ. In our analysis we fit the central values [24]: $M_Z = 91.188\,\text{GeV}$, $M_W = 80.419\,\text{GeV}$, $G_\mu \times 10^5 = 1.1664\,\text{GeV}^{-2}$, $\alpha_{EM}^{-1} = 137.04$, $M_\tau = 1.7770\,\text{GeV}$ with 0.1% numerical uncertainties; and the following with the experimental uncertainty in parentheses: $\alpha_s(M_Z) = 0.1172\,(0.0020)$, $\rho_{\rm NEW} \times 10^3 = -0.200\,(1.1)$ [25], $M_t = 178.0\,(4.3)$ GeV, $m_b(m_b) = 4.20\,(0.20)$ GeV.[4] We include the complete one loop threshold corrections at M_Z to all observables. In addition we use one loop QED and three loop QCD RG running below M_Z.

The output of this analysis is a set of weak scale squark, slepton, gaugino and Higgs masses. With regards to the calculated Higgs and sparticle masses, the neutral Higgs masses h, H, A are pole masses calculated with the leading top, bottom, stop, sbottom loop contributions; while all other sparticle masses are running masses. This output is then used to compute the cosmological dark matter density of the lightest neutralino $\Omega_\chi h^2$, which is the LSP, the branching ratio ${\rm BR}(B_s \to \mu^+\,\mu^-)$, and other observables, as described in more detail below. Note, it is important to emphasize that neither $\Omega_\chi h^2$ nor the branching ratio ${\rm BR}(B_s \to \mu^+\,\mu^-)$ are included in the χ^2 analysis. They are predictions of the model obtained in the regions selected by consistency with gauge coupling and third generation Yukawa unification and the low energy observables.

Using χ^2 penalties[5] we apply two additional constraints:

- $m_{\tilde{t}_1} \geq 300\,\text{GeV}$

[3] Note, we have checked that switching to 2 loop RGEs for dimensionful parameters can be compensated for by small changes in the GUT scale parameters, without significant changes in the low energy results.

[4] Note we take a conservative error for $m_b(m_b)$ [24] in view of recent claims to much smaller error bars [26].

[5] In order to constrain the values of some physical observables in our χ^2 analysis, such as $m_{\tilde{t}_1}$ or m_A, we add a significant contribution to the χ^2 function for values of these observables outside the desired range. We refer to this additional contribution as a χ^2 penalty. Minimization of χ^2 with Minuit, then pushes the fits to the desired range. Of course the χ^2 penalties then vanish.

JHEP09(2005)029

- m_A fixed.

The first is chosen to be consistent with $\mathrm{BR}(B \to X_s\gamma)$ [3]. Note, although we do calculate $\mathrm{BR}(B \to X_s\gamma)$, we do not use it as a constraint in the analysis. This is for two reasons — 1) this decay mode depends on 3-2 generation mixing which is model dependent and 2) it is not difficult to fit $\mathrm{BR}(B \to X_s\gamma)$ for large enough values of $m_{\tilde{t}_1}$. Hence, in order to be generally consistent with the measured value of $\mathrm{BR}(B \to X_s\gamma)$, we impose $m_{\tilde{t}_1} \geq 300\,\mathrm{GeV}$. With regards to the second constraint, since $\Omega_\chi h^2$ and $\mathrm{BR}(B_s \to \mu^+\,\mu^-)$ are both sensitive to the value of m_A, we fix its value and present our results for different values of m_A.[6]

Finally, after performing the χ^2 analysis, we impose the following constraints on the parameter space:

- lower bound on the lightest chargino mass $m_{\chi^+} > 104\,\mathrm{GeV}$;
- lower bound on the light Higgs mass $m_h > 111\,\mathrm{GeV}$. Note, because of the theoretical uncertainty in the calculation of m_h ($\sim 3\,\mathrm{GeV}$), we conservatively impose $m_h > 111\,\mathrm{GeV}$, instead of the LEP bound for SM Higgs $m_h > 114.4\,\mathrm{GeV}$;
- branching ratio $\mathrm{BR}(B_s \to \mu^+\,\mu^-)$. The current best published limit comes from DZero $\mathrm{BR}(B_s \to \mu^+\,\mu^-) < 5.0 \times 10^{-7} (4.1 \times 10^{-7})$ at 95% (90%) CL [7]. Recently CDF has announced a new preliminary bound $< 2.0 \times 10^{-7}$ at 95% CL [8], while DZero has come up with a new preliminary bound $< 3.7 \times 10^{-7}$ at 95% CL [9]. We'll discuss the impact of the bounds below;
- the relic abundance of the lightest neutralino in the range $0.094 < \Omega_\chi h^2 < 0.129$ ($2\,\sigma$) which we take as a preferred range. We will exclude points for which $\Omega_\chi h^2 > 0.129$ but allow for the possibility that $\Omega_\chi h^2 < 0.094$ (subdominant component of cold DM).

The quantity $\mathrm{BR}(B_s \to \mu^+\,\mu^-)$ is computed assuming the CKM mixings among squarks (minimal flavor violation). For this purpose we use leading log expressions derived in the first paper of ref. [6]. The SM prediction is around 3×10^{-9} while SUSY contributions to the process are dominated by pseudoscalar exchange and scale as $\tan^6\beta/m_A^4$, and can be large. Note, the branching ratio also depends on the (model dependent) 3-2 generation squark mixings. However, the mixings tend to increase $\mathrm{BR}(B_s \to \mu^+\,\mu^-)$ which make our lower bound on m_A stronger. On the other hand, beyond leading log corrections can relax our bounds on m_A by up to $\mathcal{O}(20\%)$ because of a "focusing effect" [17, 18], especially if the squark mixings are non-minimal.

We compute the relic abundance $\Omega_\chi h^2$ of the lightest neutralino using exact expressions for neutralino pair annihilation into all allowed final-state channels, which are valid both near and further away from resonances and thresholds [27]. We further treat the neutralino

[6]The calculation of $\mathrm{BR}(B \to X_s\gamma)$ and $\mathrm{BR}(B_s \to \mu^+\,\mu^-)$ requires a model for fermion mass matrices. In the absence of such a model we use the observed CKM matrix elements to calculate these flavor violating branching ratios.

JHEP09(2005)029

coannihilation with the lightest chargino and next-to-lightest neutralino [28] and with the lighter stau [29] with similar precision. We include all coannihilation channels, including the previously neglected [2] coannihilation with light stops, although this channel only affects points in the parameter space which are excluded by other constraints. We solve the Boltzmann equation numerically as in [30] and compute $\Omega_\chi h^2$ with an error of a few per cent, which is comparable with today's accuracy on the observational side.

3. Results

In figures 1, 2 and 3 we present our results for different values of m_{16} and m_A in the μ, $M_{1/2}$ plane. For example, in figure 1 we present, for $m_{16} = 3\,\mathrm{TeV}$ and $m_A = 500\,\mathrm{GeV}$ (left panel) and $m_A = 700\,\mathrm{GeV}$ (right panel) the (magenta) solid lines of constant χ^2. The red (lightest shaded) regions are excluded by collider limits and by $\Omega_\chi h^2 > 0.129$. Specifically the red regions at small μ and/or small $M_{1/2}$ (bounded by the solid black line) is excluded by bounds on the chargino mass $m_\chi > 104\,\mathrm{GeV}$ and the red region on the right side (bounded by the dashed black line) is excluded by (our conservative application of) the LEP Higgs bound $m_h > 111\,\mathrm{GeV}$. The cosmologically preferred dark matter region green (darkest shaded) satisfy $0.094 < \Omega_\chi h^2 < 0.129$. We find significant regions of parameter

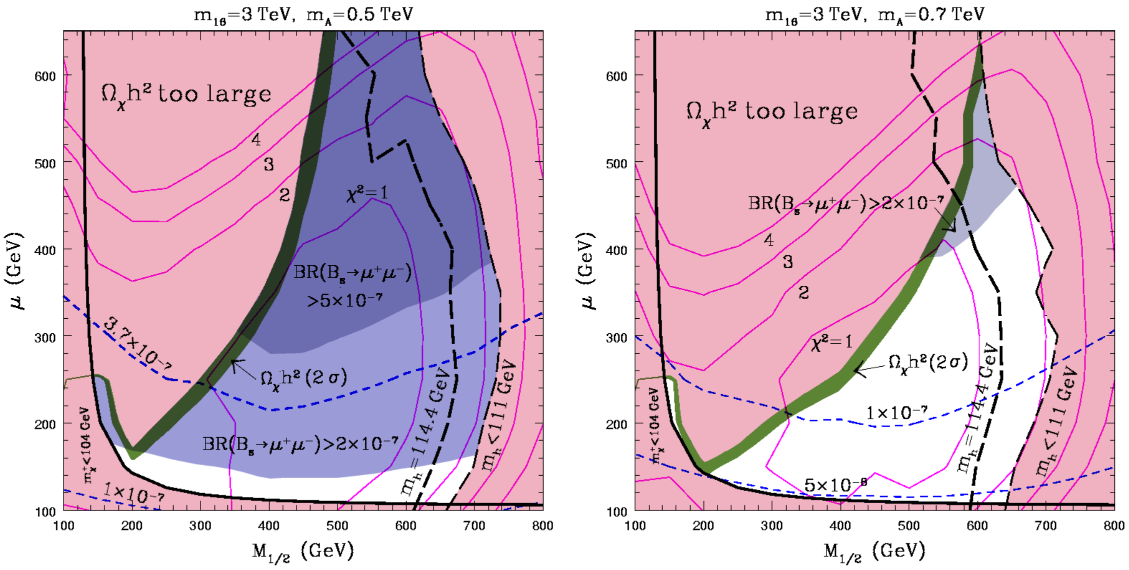

Figure 1: Contours of constant χ^2 for $m_{16} = 3\,\mathrm{TeV}$ and $m_A = 500\,\mathrm{GeV}$ (left panel) and $700\,\mathrm{GeV}$ (right panel). The red (light shaded) regions are excluded by $m_{\chi^+} < 104\,\mathrm{GeV}$ (below and to the left of the solid black curve), $m_h < 111\,\mathrm{GeV}$ (on the right) and by $\Omega_\chi h^2 > 0.129$. To the right of the thick broken black line one has $m_h < 114.4\,\mathrm{GeV}$. The green (darkest shaded) band corresponds to the preferred $2\,\sigma$ range $0.094 < \Omega_\chi h^2 < 0.129$, while the white regions below it correspond to $\Omega_\chi h^2 < 0.094$. The region excluded by the DZero experimental bound on $\mathrm{BR}(B_s \to \mu^+\mu^-) < 5.0 \times 10^{-7}$ at 95% CL is marked in dark blue (dark shaded), while the region affected by the new preliminary CDF bound $< 2.0 \times 10^{-7}$ at 95% is marked in light blue (light shaded). Contours of constant $\mathrm{BR}(B_s \to \mu^+\mu^-)$ are given by the blue dashed lines.

JHEP09(2005)029

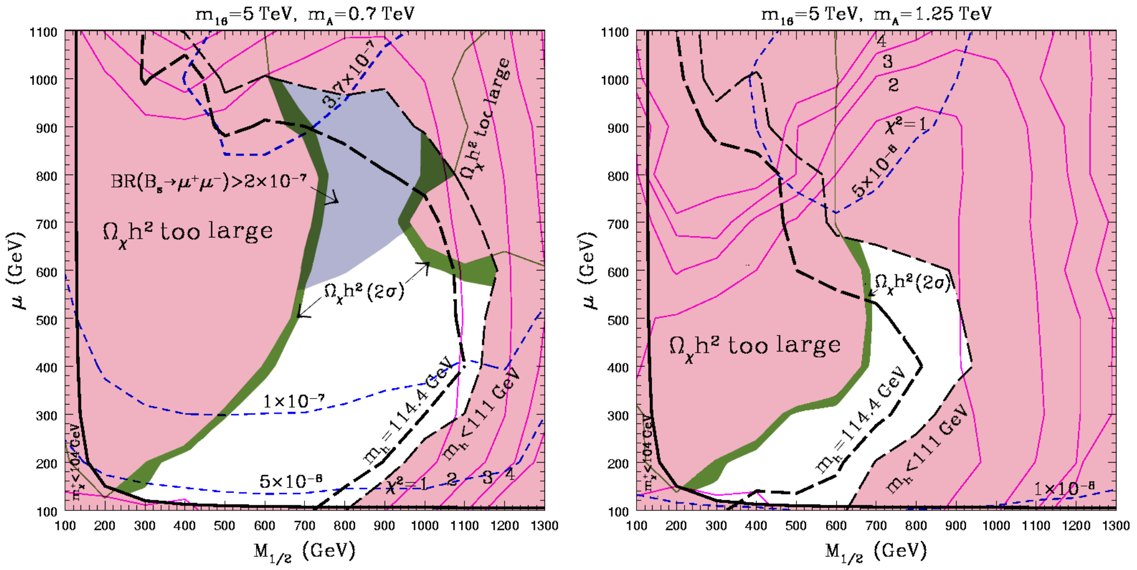

Figure 2: Same as figure 1 for $m_{16} = 5\,\mathrm{TeV}$ and $m_A = 700\,\mathrm{GeV}$ (left window) and $1250\,\mathrm{GeV}$ (right window).

space which give $\chi^2 \leq 3$, satisfy the preferred $\Omega_\chi h^2$ range as above, and satisfy all other phenomenological constraints. In figure 2, we have $m_{16} = 5\,\mathrm{TeV}$ and $m_A = 700$ and $1250\,\mathrm{GeV}$, respectively, and in figure 3 we have $m_{16} = 3$ and $5\,\mathrm{TeV}$, respectively, and $m_A = 1\,\mathrm{TeV}$.

In figure 1, marked in dark blue (dark shaded), is the region excluded by the DZero experimental bound on $\mathrm{BR}(B_s \to \mu^+\,\mu^-) < 5.0 \times 10^{-7}$ at 95% CL [7] and, in figures 1 and 2, light blue (light shaded) is the region affected by the new preliminary CDF bound $< 2.0 \times 10^{-7}$ at 95% CL [8]. In addition, we have included contours of constant $\mathrm{BR}(B_s \to \mu^+\,\mu^-)$ with dashed blue lines. The branching ratio $\mathrm{BR}(B_s \to \mu^+\,\mu^-)$ is sensitive to the value of the CP odd Higgs mass m_A [5], scaling as m_A^{-4}. For $m_A = 500\,\mathrm{GeV}$ (figure 1 (left)) the branching ratio $\mathrm{BR}(B_s \to \mu^+\,\mu^-)$ is below the published DZero bound, for acceptable values of $\Omega_\chi h^2$ and $\chi^2 < 3$, but is almost excluded by the preliminary CDF bound. While for $m_A = 1.25\,\mathrm{TeV}$ (see figure 2 (right window)) we have $\mathrm{BR}(B_s \to \mu^+\,\mu^-) > 10^{-8}$.

The cosmological relic abundance of the neutralino $\Omega_\chi h^2$ is primarily determined by the direct s-channel pair-annihilation into SM fermion pairs through the CP odd Higgs. Since all the sfermions are very heavy, their contribution to reducing the neutralino number density is strongly suppressed. In contrast, because of the coupling $Ab\bar{b} \propto \tan\beta$ (and similarly for the τ's), the A-resonance is effective and broad. Near $m_\chi \approx m_A/2$ it reduces $\Omega_\chi h^2$ down to allowed but uninterestingly small values $\ll 0.1$. As one moves away from the resonance, $\Omega_\chi h^2$ grows, reaches the preferred range $0.094 < \Omega_\chi h^2 < 0.129$, before becoming too large $\Omega_\chi h^2 > 0.129$.[7] (A similar, but much more narrow resonance due to h^0

[7] Note that at one loop we have $M_1(M_Z) = M_{1/2} * \alpha_1(M_Z)/\alpha_G$ so $M_1(M_Z) \approx 0.4 M_{1/2}$. For bino-like neutralino (which is true for larger μ), we thus have $m_\chi \approx 0.4 M_{1/2}$. Hence for s-channel annihilation we have $m_A \approx 2 m_\chi \approx 0.8\ M_{1/2}$ or $M_{1/2} \approx (5/4)\, m_A$ for the position of the "peak suppression."

JHEP09(2005)029

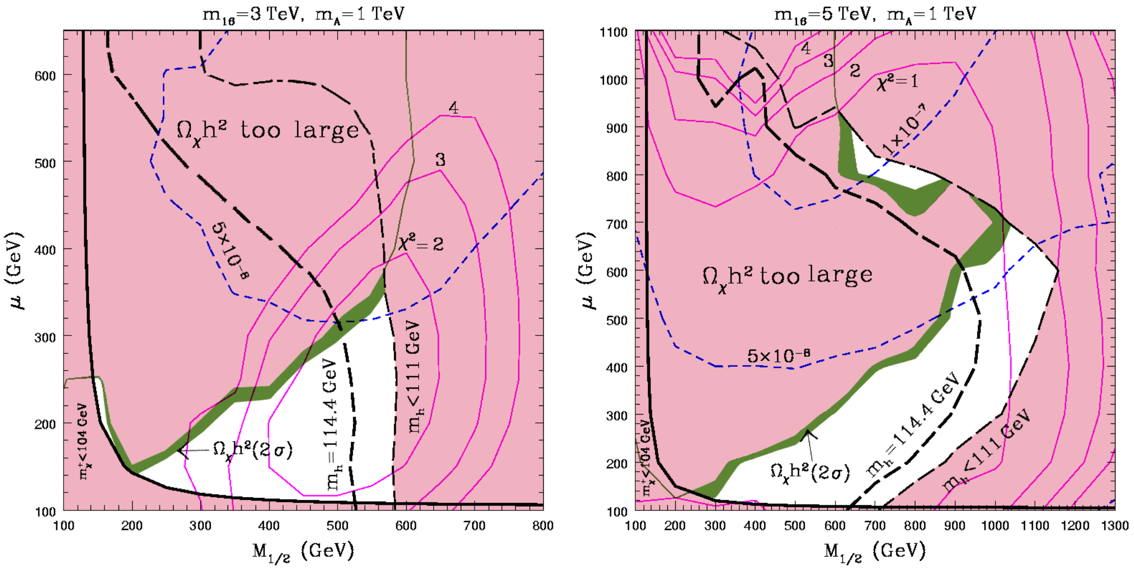

Figure 3: Same as figure 1 for $m_{16} = 3\,\text{TeV}$ (left window) $5\,\text{TeV}$ (right window) and $m_A = 1$ TeV.

is also present at $M_{1/2} \approx 150\,\text{GeV}$ and small μ.) When $m_\chi \gtrsim m_t$ ($M_{1/2} \gtrsim 420\,\text{GeV}$) and the stops are not too heavy, the LSP pairs annihilate to $t\,\bar{t}$-pairs. In the region of large $M_{1/2}$, often where m_h is already too low, two additional channels become effective. First, in this region the neutralino becomes almost mass degenerate with the lighter stau which leads to reducing $\Omega_\chi h^2$ through coannihilation. Second, if m_A is not too large, neutralino pair-annihilation into Higgs boson pairs AA and HH opens up. Finally, at $\mu \ll M_{1/2}$, the relic abundance is strongly reduced due to the increasing higgsino component of the LSP.

3.1 Experimental tests

$BR(B_s \to \mu^+\mu^-)$: as we see in figures 1–2, the preliminary Tevatron limit on $BR(B_s \to \mu^+\mu^-)$ puts a significant lower bound on $m_A \gtrsim 500\,\text{GeV}$. The dependence on m_A is plotted in figure 4 with points in the preferred region with all the collider constraints satisfied, $\chi^2 < 3$ and $0.094 < \Omega_\chi h^2 < 0.129$, for the two representative cases $m_{16} = 3$ and $5\,\text{TeV}$. Note that, for a fixed value of m_A, a vertical spread of points is caused by the changing shape of the cosmologically favored band in the μ, $M_{1/2}$ plane and some variation in $\tan\beta$ in figures 1–3.

We now argue that there is an upper bound on m_A, the CP odd Higgs mass. Hence there is a lower bound on the branching ratio $BR(B_s \to \mu^+\mu^-)$. We first show that increasing the value of m_{16} permits a larger range for the parameters μ, $M_{1/2}$. Comparing figures 1–3 we see that, as m_{16} increases, the region with $\chi^2 < 3$ rapidly grows. Note, the dominant pull in χ^2 is due to the bottom quark mass. In order to fit the data, the total SUSY corrections to $m_b(m_b)$ must be of order $-(2-4)\%$ [3]. In addition there are three dominant contributions to these SUSY corrections: a gluino loop contribution $\propto\ \alpha_3\ \mu\ M_{\tilde{g}}\ \tan\beta/m^2_{\tilde{b}_1}$, a chargino loop contribution $\propto\ \lambda_t^2\ \mu\ A_t\ \tan\beta/m^2_{\tilde{t}_1}$, and a term $\propto\ \log M^2_{\rm SUSY}$. Larger values of m_{16} permit a larger range for the ratio $m_{\tilde{b}_1}/m_{\tilde{t}_1}$. *Thus larger*

JHEP09(2005)029

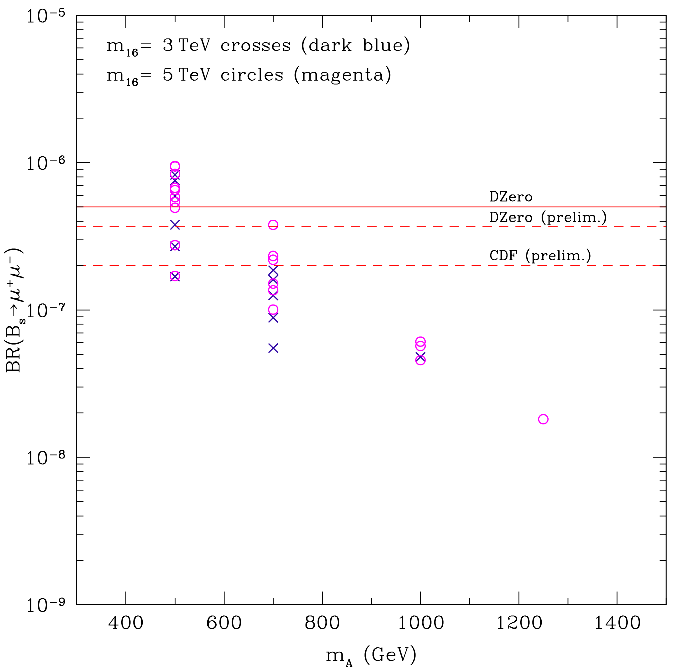

Figure 4: The branching ratio $\mathrm{BR}(B_s \to \mu^+ \mu^-)$ as a function of m_A in the μ, $M_{1/2}$ region of parameter space satisfying all the collider constraints, $0.094 < \Omega_\chi h^2 < 0.129$ and $\chi^2 < 3$ for fixed $m_{16} = 3$ and 5 TeV.

values of m_{16} allows more freedom in parameter space for fitting the data at both smaller or larger values of μ, $M_{1/2}$. Note, also when m_{16} increases (with $M_{1/2}$ fixed) the parameter A_t becomes more negative, since $A_0 \approx -2\ m_{16}$ and $A_t \approx -3\ M_{1/2} + \epsilon\ A_0$ where $\epsilon \ll 1$.

In addition, as $M_{1/2}$ increases the light Higgs mass decreases. The reason for this can easily be seen. Consider the approximate equation for the light Higgs mass (eq. (2.32) from ref. [23])[8]

$$\begin{aligned} m_h^2 \approx M_Z^2 &\left(1 - \frac{3}{8\pi^2}\frac{m_t(m_t)^2}{v^2}t\right) + \\ &+ \frac{3}{4\pi^2}\frac{m_t(m_t)^4}{v^2}\left[\frac{1}{2}\tilde{X}_t + t + \frac{1}{16\pi^2}\left(\frac{3}{2}\frac{m_t(m_t)^2}{v^2} - 32\pi\alpha_3\right)(\tilde{X}_t t + t^2)\right] \end{aligned} \tag{3.1}$$

where

$$\tilde{X}_t = \frac{2A_t^2}{M_{\mathrm{SUSY}}^2}\left(1 - \frac{A_t^2}{12M_{\mathrm{SUSY}}^2}\right), \qquad t = \log\left(\frac{M_{\mathrm{SUSY}}^2}{m_t(m_t)^2}\right)$$

and

$$M_{\mathrm{SUSY}} \approx \sqrt{\frac{(m_{\tilde{t}_1}^2 + m_{\tilde{t}_2}^2)}{2}}\,.$$

In our analysis, the bottom quark gets a positive supersymmetric correction proportional

[8]This approximation gives a value for the light Higgs mass which is larger than the value obtained with a more exact calculation (see figure 2 in ref. [23]) for values of $|A_t|$ above 2 TeV. The discrepancy increases with increasing $|A_t| \geq 2$ TeV, overestimating the Higgs mass by as much as 8 GeV for $|A_t| = 3.6$ TeV.

to $\mu M_{1/2}$ and a negative contribution proportional to μA_t. Thus in order to fit the bottom quark mass as $M_{1/2}$ increases, $-A_t$ also increases. As a consequence, in the relevant region of parameter space, $\tilde{X}_t$ decreases. In addition, the fit value of $m_t(m_t)$ also decreases. *Hence the value of m_h decreases as $M_{1/2}$ increases.* Furthermore, at fixed values of $M_{1/2}$ the light Higgs mass m_h decreases as m_A increases. On the other hand, the value of the light Higgs mass is fairly insensitive to m_{16}.[9] In the acceptable regions of parameter space we find $114.4 < m_h < 121\,\text{GeV}$.[10]

Now let us put it all together. Comparing various windows in figures 1–3, we see that increasing m_A has two effects. It suppresses the branching fraction $\text{BR}(B_s \to \mu^+\,\mu^-)$. At the same time it moves the s-channel neutralino annihilation channel to larger values of $M_{1/2}$; providing larger regions with $0.094 < \Omega_\chi h^2 < 0.129$. However, increasing m_A above 1 TeV or so moves the regions of preferred $\Omega_\chi h^2$ too far to the right, in potential conflict with a lower bound on m_h. In fact, as can be seen from figure 2 (lower right), *there is a rough upper bound on m_A of about 1.3 TeV (and a corresponding lower bound on* $\text{BR}(B_s \to \mu^+\,\mu^-) > \mathcal{O}(10^{-8})$),[11] above which there are no longer any solutions consistent with the observed $\Omega_\chi h^2$ and the lower bound on the Higgs mass.

It has been shown that, with an integrated luminosity of $15\,\text{fb}^{-1}$, experiments at the Tevatron are sensitive to $\text{BR}(B_s \to \mu^+\,\mu^-) > 1.2\times10^{-8}$ [31]. Hence this offers the prospect of a full exploration of the model in this observable. In addition, the LHC is expected to be sensitive down to $(3.5 \pm 1.0) \times 10^{-9}$ [32]. We discuss $BR(B_s \to \mu^+\mu^-)$ further below.

WIMP direct detection search. We begin by plotting in figure 5 σ_p^{SI}, the spin independent neutralino dark matter cross section relevant for direct dark matter searches, versus m_A. We show the cases $m_{16} = 3\,\text{TeV}$, $m_A = 500,\ 700,\ 1000\,\text{GeV}$ (dark blue crosses) and $m_{16} = 5\,\text{TeV}$, $m_A = 500,\ 700,\ 1000,\ 1250\,\text{GeV}$ (magenta circles). The points lie in the preferred region with all the collider constraints satisfied, $\chi^2 < 3$ and $0.094 < \Omega_\chi h^2 < 0.129$. Like in figure 4, for a fixed value of m_A, a vertical spread of points is caused by the changing shape of the cosmologically favored band in the μ, $M_{1/2}$ plane and also by some variation in $\tan\beta$ in figures 1–3. The dominant contribution to both tree-level and one-loop diagrams typically comes from a t-channel exchange of the heavier scalar Higgs boson H^0. Thus one would normally expect $\sigma_p^{SI} \sim m_A^{-4}$ since $m_A \simeq m_H$. However, the coupling $\chi\chi H^0$ is sensitive to the bino/higgsino composition of the lightest neutralino and vanishes in the limit of the neutralino becoming one of these two states. The bino fraction increases along the cosmologically favored band from as low as some 70% at low μ to almost 100% at largest allowed μ. This causes σ_p^{SI} to decrease with μ even for a fixed m_A.

Since both $BR(B_s \to \mu^+\mu^-)$ and σ_p^{SI} are to a large degree determined by m_A, but also by the LSP composition, one finds interesting correlations which are shown in figure 6. The small light points obey all collider constraints and $\chi^2 < 3$, while the larger dark

[9]Although for fixed $M_{1/2}$ the light Higgs mass does increase by a small amount as m_{16} increases (see figure 3).

[10]Note, there is at least a $\pm 3\,\text{GeV}$ theoretical uncertainty in the Higgs mass.

[11]The upper bound on m_A will increase slightly as m_{16} increases, but then m_{16} cannot increase significantly without creating a fine-tuning problem.

JHEP09(2005)029

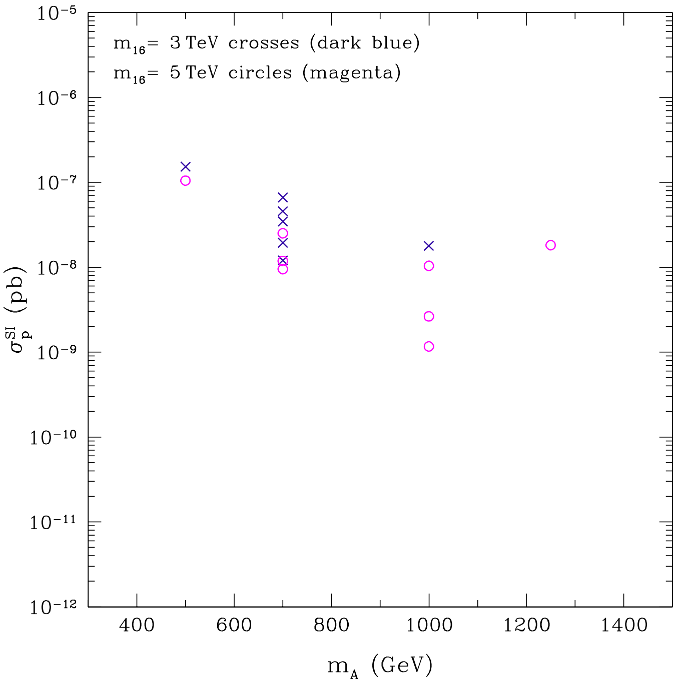

Figure 5: Spin independent neutralino dark matter cross section σ_p^{SI} versus m_A for $m_{16} = 3\,\mathrm{TeV}$ (dark blue crosses) and $5\,\mathrm{TeV}$ (magenta circles). The points obey all collider constraints, $\chi^2 < 3$, $0.094 < \Omega_\chi h^2 < 0.129$ and the new preliminary CDF bound $\mathrm{BR}(B_s \to \mu^+ \mu^-) < 2.0 \times 10^{-7}$.

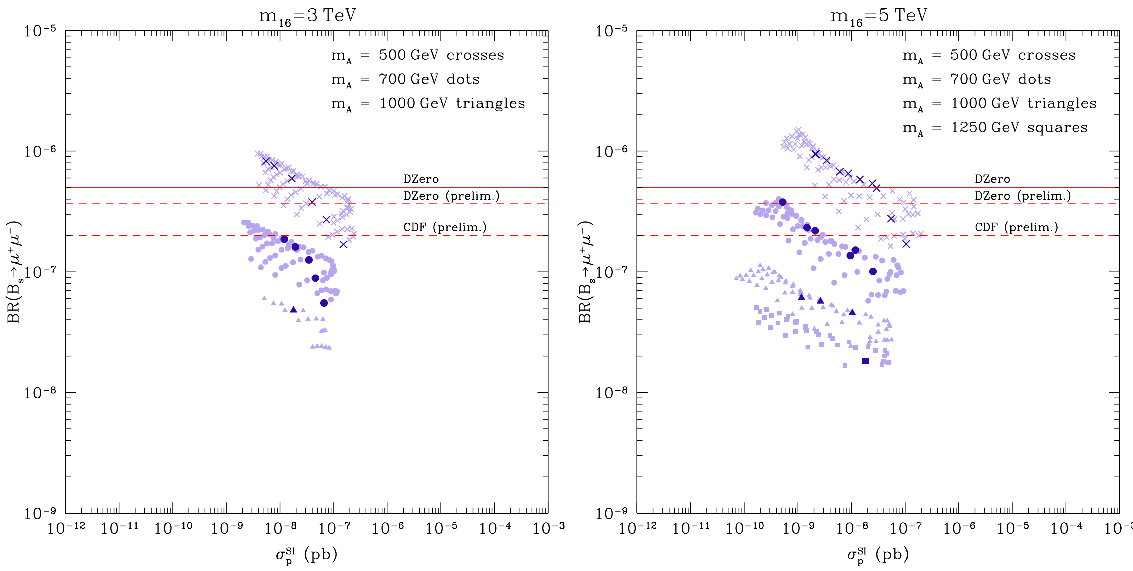

Figure 6: The branching ratio $\mathrm{BR}(B_s \to \mu^+ \mu^-)$ versus spin independent neutralino dark matter cross section σ_p^{SI} for $m_{16} = 3\,\mathrm{TeV}$ (left window) and $5\,\mathrm{TeV}$ (right window) and for several choices of m_A. The small light points obey all collider constraints and $\chi^2 < 3$, while the larger dark points satisfy in addition $0.094 < \Omega_\chi h^2 < 0.129$.

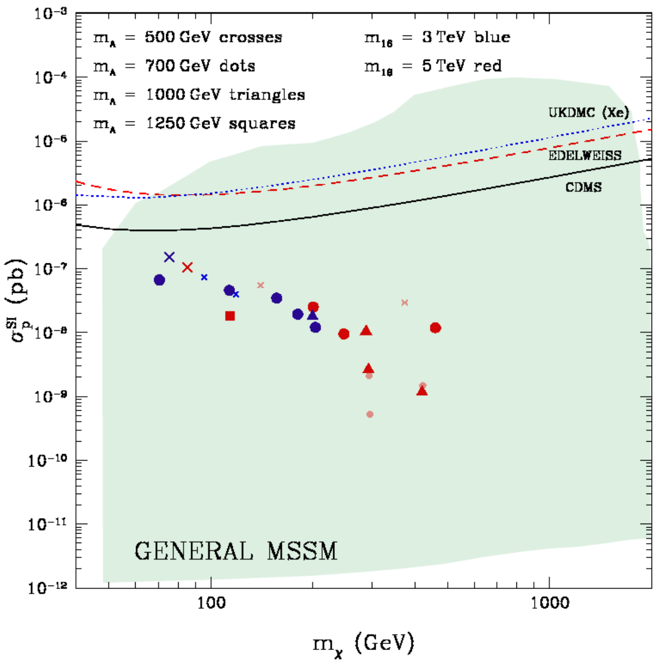

Figure 7: Spin independent dark matter cross section σ_p^{SI} vs. the neutralino mass m_χ for several choices of m_{16} and m_A. Big points obey all collider constraints, $\chi^2 < 3$, $0.094 < \Omega_\chi h^2 < 0.129$ and the new preliminary CDF bound $\mathrm{BR}(B_s \to \mu^+ \mu^-) < 2.0 \times 10^{-7}$ while for the small, light points the last constraint is relaxed to $\mathrm{BR}(B_s \to \mu^+ \mu^-) < 5.0 \times 10^{-7}$. The lightly shaded background represents predictions in the general MSSM for which the bound from $\mathrm{BR}(B_s \to \mu^+ \mu^-)$ was not applied.

points satisfy in addition $0.094 < \Omega_\chi h^2 < 0.129$. For fixed m_A and $M_{1/2}$, σ_p^{SI} decreases with increasing μ due to the increasing bino content of the neutralino. On the other hand $\mathrm{BR}(B_s \to \mu^+ \mu^-)$ increases as μ increases, since the flavor violating vertex correction is proportional to μ (see below). Hence, as seen from figure 6, in the allowed parameter space of the $\mathrm{MSO_{10}SM}$, the values for σ_p^{SI} and $\mathrm{BR}(B_s \to \mu^+ \mu^-)$ are (as one moves along the cosmologically favored band, for a fixed m_A) *inversely* correlated. This behavior sharply contrasts with the direct correlation between the two quantities in the CMSSM and its extensions presented in [33], where, with the usual parametrization, the masses of the Higgs bosons grow along the cosmologically favored band. Thus, an improved limit on $BR(B_s \to \mu^+\mu^-)$ does not need to necessarily imply less promising prospects for measuring σ_p^{SI}, and vice versa. In addition, in figure 6 we see that, comparing the case of $m_{16} = 3$ and 5 TeV (again, for fixed m_A) in the latter case the range of σ_p^{SI} for the (dark) points in the cosmologically preferred region extends to larger values of $\mathrm{BR}(B_s \to \mu^+ \mu^-)$. This is because the flavor violating vertex of the CP odd Higgs scales roughly like $\mu A_t/m_{16}^2$ and for larger values of m_{16} the acceptable regions of parameter space extend to even larger values of μ.

In figure 7 we plot σ_p^{SI} versus the neutralino mass. We show the same cases of m_{16} and m_A as in figures 4–6. Big points obey all collider constraints, $\chi^2 < 3$, $0.094 < \Omega_\chi h^2 < 0.129$ and the new preliminary CDF bound $\mathrm{BR}(B_s \to \mu^+ \mu^-) < 2.0 \times 10^{-7}$ while for the small, light points the last constraint is relaxed to $\mathrm{BR}(B_s \to \mu^+ \mu^-) < 5.0 \times 10^{-7}$. In the (light

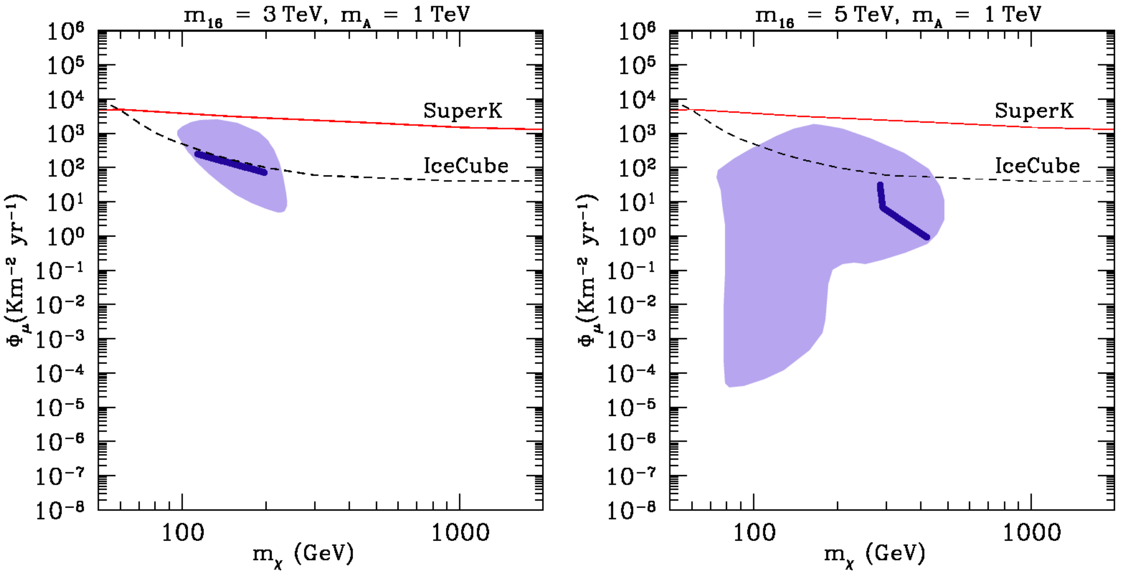

Figure 8: Muon flux from the Sun vs. the neutralino mass m_χ for $m_A = 1\,\mathrm{TeV}$ and $m_{16} = 3\,\mathrm{TeV}$ (left window) and $m_{16} = 5\,\mathrm{TeV}$ (right window) assuming the energy threshold $E_\mu^{\mathrm{th}} = 25\,\mathrm{GeV}$. In light blue (shaded) areas the collider constraints and $\chi^2 < 3$ have been applied but not the cosmological constraint $0.094 < \Omega_\chi h^2 < 0.129$ nor the bound on $\mathrm{BR}(B_s \to \mu^+\mu^-)$. Points along the dark blue line additionally satisfy the cosmologically preferred range $0.094 < \Omega_\chi h^2 < 0.129$. The current limit from SuperKamiokande is marked as a red solid line while future reach of IceCube is marked as a black dashed line.

blue) background we plot predictions obtained in the general MSSM by scanning large ranges of parameters, including $\tan\beta$ from 10 up to 65 [34] but do not apply the bound from $\mathrm{BR}(B_s \to \mu^+\mu^-)$. Note, most regions of parameter space should be observable as dark matter search experiments are expected to probe down to values of $\sigma_p^{SI} \gtrsim 10^{-8}$ pb with current/upgraded detectors within the next year or so (e.g., by CDMS). Future one-tonne detectors are planned to reach $\sigma_p^{SI} \gtrsim 10^{-10}$ pb, thus probing the entire favored parameter space of the MSO$_{10}$SM.

WIMP indirect detection search. Apart from direct detection, dark matter WIMP signals can be detected in a number of indirect detection search channels. Here we compute detection rates for a high-energy neutrino flux from the Sun, for gamma rays from the Galactic center, and for antiprotons and positrons from the Galactic halo, by applying DARKSUSY [30] to some popular Galactic halo models. As we will see, prospects for WIMP detection in these modes are generally less promising than in direct detection experiments, although a sizeable number of cosmologically preferred cases can still be probed. On top of this, astrophysical uncertainties are often sizeable, especially for the latter two modes since propagation of antiprotons and positrons in the Milky Way is poorly understood.

Instead of undertaking a full presentation of all the cases discussed above, we will select a representative value of $m_A = 1\,\mathrm{TeV}$ and will present our results assuming all collider constraints (except for the $\mathrm{BR}(B_s \to \mu^+\mu^-)$ bound which, for the chosen value of m_A, is irrelevant), $\chi^2 < 3$ and $\Omega_\chi h^2 < 0.129$, and then show the (typically strong) impact of imposing the cosmological constraint $0.094 < \Omega_\chi h^2 < 0.129$. Whenever the WIMP relic density is too small ($\Omega_\chi h^2 < 0.094$), we will not rescale the rates.

Halo WIMPs pass through the Sun and other celestial bodies and occasionally become gravitationally trapped inside their cores. Once enough of them have accumulated, they start pair-annihilating into pairs of SM particles ($q\bar{q}$, WW, ZZ, etc), which subsequently decay via two– and three-body processes, like $b \to c l \nu_l$, $W \to \bar{\nu}\nu$, etc. Among the decay products only neutrinos can escape out of the Sun's core. A muon neutrino from the Sun, when passing through the Earth, may produce a muon which will generate a Čerenkov shower in a nearby under-ice or under-water detector.

The calculation of the WIMP capture rate and subsequent annihilation, as well as propagation of decay products is rather well understood [35] and fairly insensitive to the choice of a Galactic halo model. (We assume the local dark matter density $\rho_0 = 0.3\,\mathrm{GeV/cm^3}$ and a Maxwellian velocity distribution with the peak velocity $v_0 = 270$ km/s.) The capture rate in the Sun, typically determined by spin dependent interactions involving Z-boson exchange, is basically independent of m_A. On the other hand, the shape of the cosmologically favored band in the μ, $M_{1/2}$ plane does depend on m_A.

In figure 8 we plot the high-energy muon flux from the Sun for $m_A = 1\,\mathrm{TeV}$, and $m_{16} = 3\,\mathrm{TeV}$ (left window) and $m_{16} = 5\,\mathrm{TeV}$ (right window). The IceCube energy threshold $E_\mu^{\mathrm{th}} = 25\,\mathrm{GeV}$ has been applied. In light blue (shaded) areas the collider constraints and $\chi^2 < 3$ have been applied but not the cosmological constraint $0.094 < \Omega_\chi h^2 < 0.129$ nor explicitly the bound on $\mathrm{BR}(B_s \to \mu^+\mu^-)$. Dark lines correspond to points which additionally satisfy the cosmologically preferred range $0.094 < \Omega_\chi h^2 < 0.129$. We can see that the favored configurations fall below the current best limit from Super-Kamiokande [19] and are on a bordeline for being probed at IceCube [36].

Predictions for the fluxes of gamma rays from the Galactic center and antiprotons and (to a lesser extent) positrons from the Galactic halo depend on the assumed halo model. Several profiles of dark matter distribution have been discussed in the literature, many of which can be parametrized by

$$\rho(r) = \rho_0 \frac{(r/r_0)^{-\gamma}}{[1+(r/a)^\alpha]^{\frac{\beta-\gamma}{\alpha}}} \left[1 + \left(\frac{r_0}{a}\right)^\alpha\right]^{\frac{\beta-\gamma}{\alpha}}, \tag{3.2}$$

where $\rho(r)$ is the radial dependence of the halo WIMP density, $\rho_0 = 0.3\,\mathrm{GeV/cm^3}$ is the local dark matter density, r_0 is our distance to the Galactic center and a is a distance scale.

Here we consider three distinct and popular choices:

- a sperically symmetric modified isothermal profile [37], for which $(\alpha, \beta, \gamma) = (2, 2, 0)$, $r_0 = 8.5\,\mathrm{kpc}$ and $a = 3.5\,\mathrm{kpc}$;
- the Navarro, Frenk and White (NFW) profile [38], for which $(\alpha, \beta, \gamma) = (1, 3, 1)$, $r_0 = 8.0\,\mathrm{kpc}$ and $a = 20\,\mathrm{kpc}$;
- the Moore, et al., profile [39], for which $(\alpha, \beta, \gamma) = (1.5, 3, 1.5)$, $r_0 = 8.0\,\mathrm{kpc}$ and $a = 28\,\mathrm{kpc}$.

JHEP09(2005)029

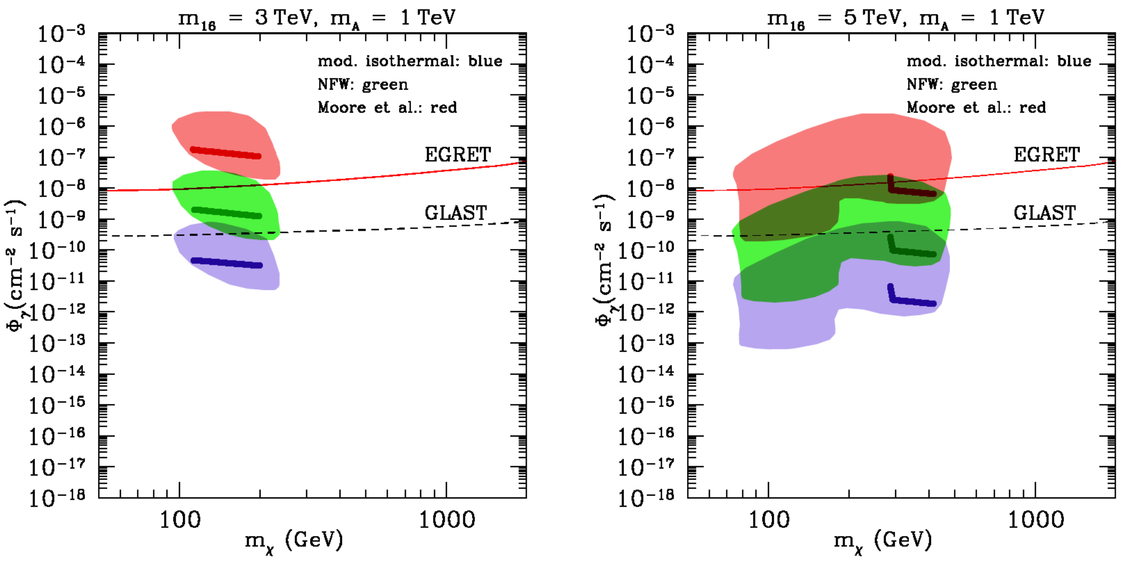

Figure 9: Gamma ray fluxes from the Galactic center vs. the neutralino mass m_χ for $m_A = 1\,\text{TeV}$ and for $m_{16} = 3\,\text{TeV}$ (left window) and $m_{16} = 5\,\text{TeV}$ (right window), assuming the energy threshold $E_\gamma^{\text{th}} = 1\,\text{GeV}$, as in GLAST. Results for three different halo models are shown, as described in the text. In light-colored (shaded) areas collider constraints and $\chi^2 < 3$ have been applied but not the cosmological constraint $0.094 < \Omega_\chi h^2 < 0.129$ nor the bound on $\text{BR}(B_s \to \mu^+\mu^-)$. Dark lines corresponding to each halo model mark points which additionally satisfy the cosmological constraint $0.094 < \Omega_\chi h^2 < 0.129$. The current limit from EGRET is marked as a red solid curve while an expected reach of GLAST is marked as a black dashed line.

Towards the Galactic center the halo density is expected to be larger than in our local neighborhood but otherwise constant in the case of the modified isothermal model, or divergent as $\rho(r) \sim 1/r$ (NFW) and $\rho(r) \sim 1/r^{1.5}$ (Moore, et al.). It is therefore natural to expect enhanced neutralino WIMP annihilations in the core of the Galactic center. Among annihilation products, high-energy gamma rays are unique in that they point back directly to the Galactic center. The flux is proportional to the DM number density squared integrated along the line of sight. Monochromatic photons with energy $E_\gamma \simeq m_\chi$ would provide a spectacular signal but the rates are low compared to the diffuse gamma radiation from cascade decays of WIMP annihilation products.

In figure 9 we plot the diffuse high-energy gamma flux from the Galactic center, integrated over the cone of 0.001 sr. We apply the continuous gamma energy threshold $E_\gamma^{\text{th}} = 1\,\text{GeV}$, as planned for GLAST [40]. We also denote an upper limit from EGRET [41] and the expected reach of GLAST after three years of taking data. The rates are independent of the choice of m_A. Depending on the choice of the halo model, GLAST may have a good chance of detecting a WIMP signal.

For comparison, in figure 10 we plot the same quantity but apply the larger energy threshold of 60 GeV, typical of HESS. For the case $m_{16} = 5\,\text{TeV}$ the cosmologically favored values of m_χ are higher than for $m_{16} = 3\,\text{TeV}$, and accordingly the resulting diffuse gamma radiation will be more accessible to HESS [42] than to GLAST. Thus HESS has a good chance of detecting a signal in the region of the parameter space which is to some extent complementary to the reach of GLAST.

JHEP09(2005)029

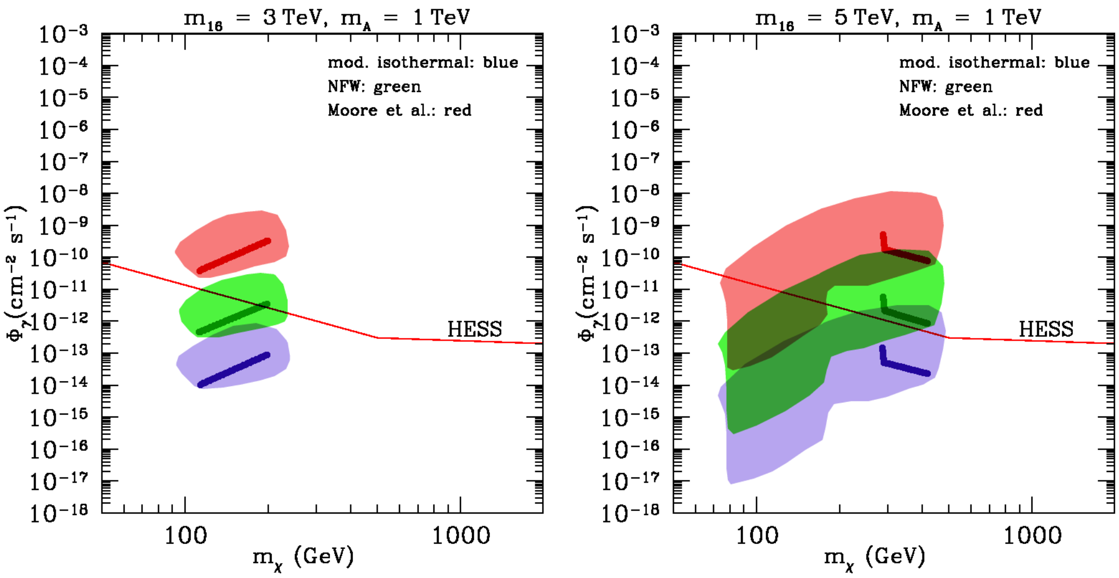

Figure 10: Same as figure 8 but assuming the energy threshold $E_\gamma^{\rm th} = 60\,{\rm GeV}$, as in HESS whose limit is marked as a red solid line.

Another way of looking for WIMPs is to look for an excess of antiparticles in cosmic rays originating from WIMP annihilation in the Galactic halo, despite large uncertainties [35, 43]. A flux of antiprotons from astrophysical sources is expected to fall off dramatically at low energies, unlike that from WIMP annihilation in the halo. For a detailed discussion of antiproton fluxes from WIMP annihilation and from background sources see ref. [43].

In figure 11 we plot a differential antiproton flux $d\,\Phi^{p^-}/dE\,d\Omega$ vs. m_χ. We evaluate the quantity assuming the peak of the flux at $E_{p^-} \sim 1.76\,{\rm GeV}$ to coincide with a peak in the kinetic energy distribution of the BESS experiment [44]. The plots do not depend on m_A and the halo model dependence is fairly weak, except for the Moore, et al., model for which the rate is somewhat higher. As we can see, the cosmologically favored points fall below the BESS sensitivity.

Finally, high energy positrons may be a signature of WIMP annihilation in the halo. Again, like in the case of antiprotons, background from astrophysical processes (mostly spallation of cosmic rays off the interstellar medium) and other astrophysical uncertainties are rather large. Production of hard positrons in e^+e^- pairs from direct WIMP annihilation is tiny due to helicity suppression. On the other hand, annihilation into WW and ZZ pairs, followed by their decays into e^+e^- pairs will result in a positron flux peaked at an energy of $\sim m_\chi/2$. This feature gives some hope of distinguishing the signal (S) due to WIMP annihilation from the background (B) which is typically two to three orders of magnitude larger.

In figure 12 we plot the signal-to-background ratio S/B. The positron flux is evaluated at an optimal energy of $m_\chi/2$ and is compared with background flux, as parametrized by Feng, et al. [45]. Halo model dependence is negligible since energetic positrons produced in the solar neighborhood would be detectable. A sensitivity of positron search experi-

JHEP09(2005)029

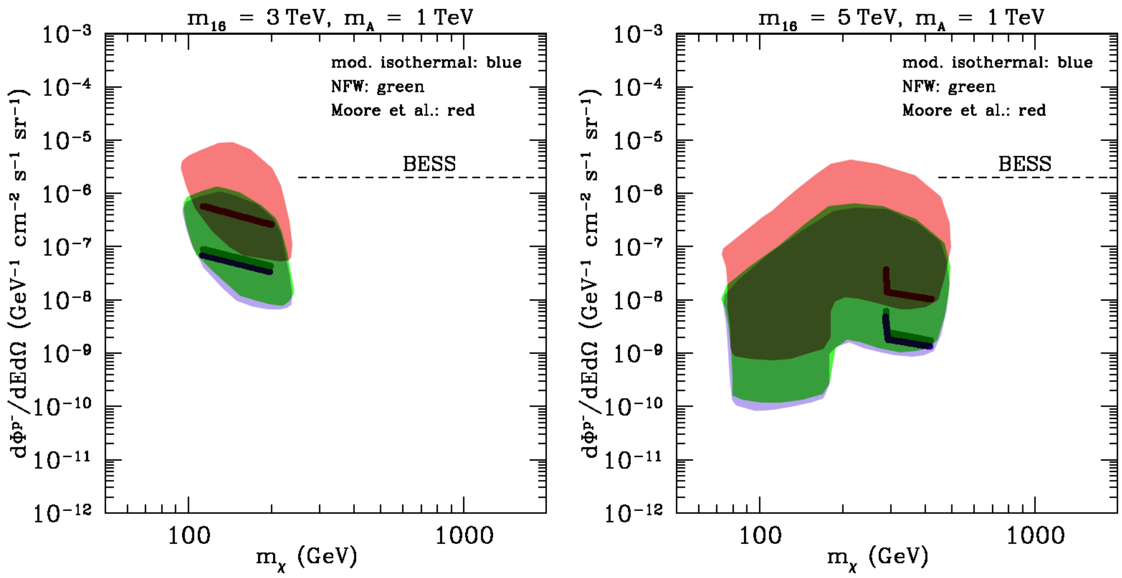

Figure 11: Same as figure 8 but for antiproton fluxes from the Galactic halo. A sensitivity of BESS is indicated with a dashed line.

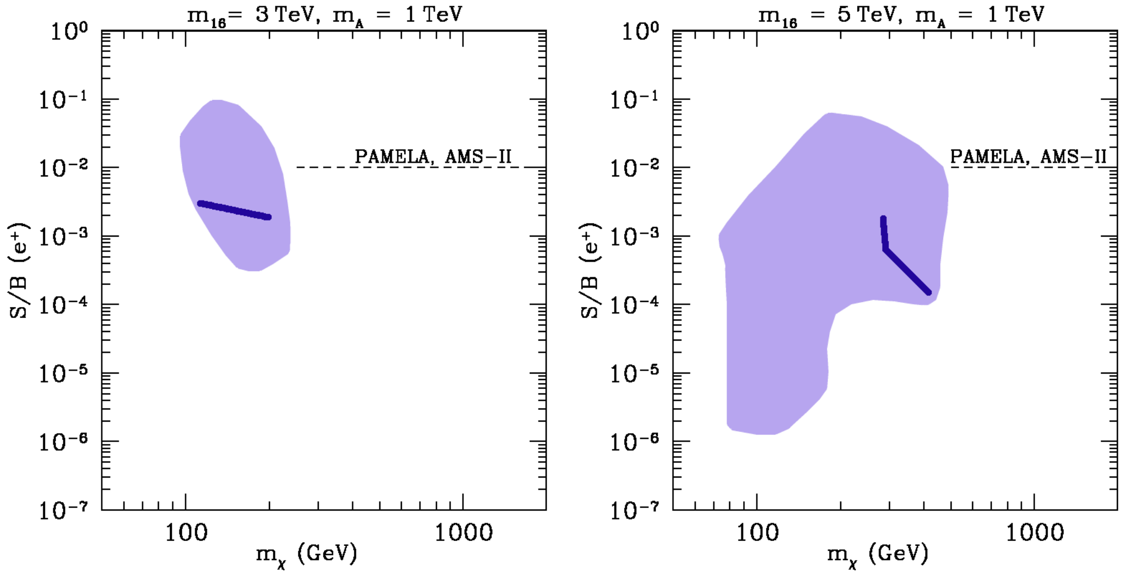

Figure 12: Same as figure 8 but for positron flux from WIMP annihilation in the Galactic halo presented as signal-to-background ratio B/S, as described in the text. Rates as low as 0.01 may be detectable at PAMELA and AMS-II.

ments PAMELA [46] and AMS-II [47] is indicated where S/B rates as low as 0.01 may be detectable. As can be seen from the figure, this is unlikely to be sufficient to probe our predicted rates for cosmologically favored regions.

3.2 Some representative points

In table 1 we present the input parameters and resulting Higgs and SUSY spectra for four representative points in SUSY parameter space which are consistent with all available data.

Data points		1	2	3	4
Input parameters					
α_G^{-1}		24.86	24.90	25.01	25.30
$M_G \times 10^{-16}$		2.96	2.82	2.59	2.30
ϵ_3		-0.036	-0.036	-0.033	-0.029
λ		0.71	0.72	0.69	0.73
m_{16}		3000	3000	3000	5000
m_{10}/m_{16}		1.33	1.35	1.37	1.35
Δm_H^2		0.15	0.17	0.16	0.16
$M_{1/2}$		330	380	500	700
μ		260	240	360	400
$\tan\beta$		51.93	51.97	50.7	51.61
A_0/m_{16}		-1.83	-1.83	-1.91	-1.88
χ^2 observables	Exp (σ)				
M_Z	91.188 (0.091)	91.19	91.19	91.19	91.22
M_W	80.419 (0.080)	80.42	80.41	80.42	80.40
$G_\mu \times 10^5$	1.1664 (0.0012)	1.166	1.166	1.166	1.166
α_{EM}^{-1}	137.04 (0.14)	137.0	137.0	137.0	137.0
$\alpha_s(M_Z)$	0.1172 (0.0020)	0.1171	0.1169	0.1171	0.1173
$\rho_{\mathrm{NEW}} \times 10^3$	-0.200 (1.10)	0.363	0.287	0.442	-0.332
M_t	178 (4.3)	176.3	176.7	175.9	177.5
$m_b(m_b)$	4.20 (0.20)	4.27	4.3	4.27	4.19
M_τ	1.7770 (0.0018)	1.777	1.777	1.777	1.777
TOTAL χ^2		0.56	0.57	0.73	0.18
h		121	121	118	119.5
H		559	791	789	1139
A		500	700	700	1000
H^+		541	758	758	1083
χ_1^0		131	148	204	287
χ_2^0		217	221	331	393
χ_1^+		214	214	328	387
$\tilde{g}$		854	979	1279	1762
$\tilde{t}_1$		300	300	300	506
$\tilde{b}_1$		690	648	716	1120
$\tilde{\tau}_1$		607	433	316	295
$a_\mu^{SUSY} \times 10^{10}$	25.6 (16)	2.95	2.91	2.75	1.04
$\Omega_\chi h^2$	$0.094 - 0.129$	0.095	0.095	0.115	0.101
$\sigma_p^{SI}(pb) \times 10^7$		0.40	0.37	0.1	0.1
$\mathrm{BR}(B_s \to \mu^+\,\mu^-) \times 10^7$	< 5	4.31	1.24	1.91	0.46
$\mathrm{BR}(B \to X_s\gamma) \times 10^4$	3.41 (0.67)	7.49	10.01	4.09	0.62

Table 1: The input parameters, χ^2 fits and Higgs and SUSY spectra for four representative points consistent with all available data.

We also present several other relevant experimental observables, including the SUSY contribution to the anomalous magnetic moment of the muon, a_μ^{SUSY}, and the branching ratio for the process $B \to X_s \gamma$, for these points. Note that one stop and/or one stau, and the charginos and neutralinos are relatively light. Also, as might be expected with heavy first and second generation sleptons, the value of a_μ^{SUSY} is small (of order 1 - 3 $\times 10^{-10}$). Finally, although BR($B \to X_s \gamma$) was not included in χ^2, and the predicted values are typically outside the experimentally allowed range, it is not difficult to find consistent solutions to all the data, including this observable.

4. Predictions and summary

This paper extends the analysis of a previous paper [2] to larger values of m_{16}, from 3 to 5 TeV, and larger CP odd Higgs mass $m_A \geq 500$ GeV. We find a well-defined, narrow region of parameter space which provides the observed relic density of dark matter, as well as a good fit to precision electroweak data, including top, bottom and tau masses, and acceptable bounds on the branching fraction of $B_s \to \mu^+ \mu^-$. We present predictions for Higgs and SUSY spectra (table 1), the dark matter detection cross section σ_p^{SI} and the branching ratio BR($B_s \to \mu^+ \mu^-$) in this region of parameter space.

The $\mathrm{MSO_{10}SM}$ predicts relatively large first and second generation scalar masses and smaller gaugino masses. An immediate consequence of such heavy first and second generation sleptons is the suppression of the SUSY contribution to the anomalous magnetic moment of the muon. We find $a_\mu^{SUSY} \leq 3 \times 10^{-10}$ (see table 1). This is consistent with the most recent experimental [48] and theoretical results at 1σ if one uses τ-based analysis [49]. However it is only consistent with an e^+e^--based analysis at 2 σ.

Another important consequence of the $\mathrm{MSO_{10}SM}$ is the large value for $\tan\beta$ which leads to an enhanced branching ratio BR($B_s \to \mu^+ \mu^-$). In addition, this is sensitive to the value of the CP odd Higgs mass m_A [5], scaling as m_A^{-4}. For $m_A = 500$ GeV, the branching ratio satisfies $2 \times 10^{-7} <$ BR($B_s \to \mu^+ \mu^-$) $< 5 \times 10^{-7}$ for acceptable values of $\Omega_\chi h^2$ and $\chi^2 < 3$.[12] In addition, we find that as m_A increases, the region of parameter space consistent with WMAP data is forced to larger values of $M_{1/2}$ and smaller values of the light Higgs mass m_h. Hence, we find an upper bound on $m_A \approx 1.3$ TeV consistent with the light Higgs mass bound $m_h > 114.4$ GeV. For $m_A \leq 1.25$ TeV, we find $BR(B_s \to \mu^+\mu^-) > 10^{-8}$. Hence all acceptable regions of parameter space lead to observable rates for BR($B_s \to \mu^+ \mu^-$).

We update our predictions for the cross section for elastic neutralino-proton scattering due to scalar interactions σ_p^{SI} as a function of the BR($B_s \to \mu^+ \mu^-$) (figure 6) and the neutralino mass (figure 7) for all regions satisfying the collider constraints, $0.094 < \Omega_\chi h^2 < 0.129$ and $\chi^2 < 3$. For comparison, in figure 7, we also show the bounds from the present dark matter searches. Over the next two to five years the experimental sensitivity is expected to gradually improve by some three orders of magnitude. This will cover large parts of the predicted ranges of σ_p^{SI}. Finally, we extend our previous analysis to include WIMP signals in indirect detection.

[12]Where the upper limit is set by the recent DZero bound.

Acknowledgments

We gratefully acknowledge the use of the GUT χ^2 analysis code developed by T. Blažek. R.D. is supported, in part, by the U.S. Department of Energy, Contract DE-FG03-91ER-40674 and the Davis Institute for High Energy Physics. R.Rda is supported by the program 'Juan de la Cierva' of the Ministerio de Educación y Ciencia of Spain. L.R. and R.RdA acknowledge support from ENTApP (European Network of Theoretical Astroparticle Physics), member of ILIAS. S.R. received partial support from DOE grant# DOE/ER/01545-862.

References

[1] G.L. Kane, C.F. Kolda, L. Roszkowski and J.D. Wells, *Study of constrained minimal supersymmetry*, *Phys. Rev.* **D 49** (1994) 6173 [hep-ph/9312272].

[2] R. Dermisek, S. Raby, L. Roszkowski and R. Ruiz De Austri, *Dark matter and* $B/s \to \mu^+\mu^-$ *with minimal* SO(10) *soft SUSY breaking*, *JHEP* **04** (2003) 037 [hep-ph/0304101].

[3] T. Blazek, R. Dermisek and S. Raby, *Predictions for Higgs and SUSY spectra from* SO(10) *Yukawa unification with* $\mu > 0$, *Phys. Rev. Lett.* **88** (2002) 111804 [hep-ph/0107097]; *Yukawa unification in* SO(10), *Phys. Rev.* **D 65** (2002) 115004 [hep-ph/0201081].

[4] See, e.g., WMAP collaboration, D.N. Spergel et al., *First year wilkinson microwave anisotropy probe (WMAP) observations: determination of cosmological parameters*, *Astrophys. J. Suppl.* **148** (2003) 175 [astro-ph/0302209].

[5] C.-S. Huang and Q.-S. Yan, $B \to X_s\tau^+\tau^-$ *in the flipped* SU(5) *model*, *Phys. Lett.* **B 442** (1998) 209 [hep-ph/9803366];
C.-S. Huang, W. Liao and Q.-S. Yan, *The promising process to distinguish supersymmetric models with large* $\tan\beta$ *from the Standard Model:* $B \to X_s\mu^+\mu^-$, *Phys. Rev.* **D 59** (1999) 11701 [hep-ph/9803460];
S.R. Choudhury and N. Gaur, *Dileptonic decay of* B_s *meson in SUSY models with large* $\tan\beta$, *Phys. Lett.* **B 451** (1999) 86 [hep-ph/9810307];
C. Hamzaoui, M. Pospelov and M. Toharia, *Higgs-mediated FCNC in supersymmetric models with large* $\tan\beta$, *Phys. Rev.* **D 59** (1999) 095005 [hep-ph/9807350];
C.-S. Huang, L. Wei, Q.-S. Yan and S.-H. Zhu, $B_s \to \ell^+\ell^-$ *in a model II 2HDM and MSSM*, *Phys. Rev.* **D 63** (2001) 114021 [hep-ph/0006250], erratum *ibid.* **64** (2001) 059902;
K.S. Babu and C.F. Kolda, *Higgs-mediated* $B0 \to \mu^+\mu^-$ *in minimal supersymmetry*, *Phys. Rev. Lett.* **84** (2000) 228 [hep-ph/9909476];
P.H. Chankowski and L. Slawianowska, $B0/d, s \to \mu^-\mu^+$ *decay in the MSSM*, *Phys. Rev.* **D 63** (2001) 054012 [hep-ph/0008046];
A. Dedes, H.K. Dreiner and U. Nierste, *Correlation of* $B/s \to \mu^+\mu^-$ *and* $(g-2)(\mu)$ *in minimal supergravity*, *Phys. Rev. Lett.* **87** (2001) 251804 [hep-ph/0108037];
G. Isidori and A. Retico, *Scalar flavour-changing neutral currents in the large-*$\tan\beta$ *limit*, *JHEP* **11** (2001) 001 [hep-ph/0110121];
A.J. Buras, P.H. Chankowski, J. Rosiek and L. Slawianowska, *Correlation between delta* M_s *and* $B/(s,d)0 \to \mu^+\mu^-$ *in supersymmetry at large* $\tan\beta$, *Phys. Lett.* **B 546** (2002) 96 [hep-ph/0207241].

[6] C. Bobeth, T. Ewerth, F. Kruger and J. Urban, *Analysis of neutral Higgs-boson contributions to the decays anti-B/s* $\to \ell^+\ell^-$ *and* $\bar{B} \to K\ell^+\ell^-$, *Phys. Rev.* **D 64** (2001) 074014 [hep-ph/0104284];
C. Bobeth, T. Ewerth, F. Kruger and J. Urban, *Enhancement of* $B(\bar{B}/d \to \mu^+\mu^-)/B(\bar{B}/s \to \mu^+\mu^-)$ *in the MSSM with minimal flavour violation and large tan beta*, *Phys. Rev.* **D 66** (2002) 074021 [hep-ph/0204225].

[7] D0 collaboration, V.M. Abazov et al., *A search for the flavor-changing neutral current decay* $B/s0 \to \mu^+\mu^-$ *in* $p\bar{p}$ *collisions at* $\sqrt{s} = 1.9$ *6-tev with the d0 detector*, *Phys. Rev. Lett.* **94** (2005) 071802 [hep-ex/0410039].

[8] See CDF web page,
http://www-cdf.fnal.gov/physics/new/bottom/050407.blessed-bsmumu/;
For the previous published result, see D. Acosta *et al.* [CDF Collaboration], CDF collaboration, D. Acosta et al., *Search for* $B/s0 \to \mu^+\mu^-$ *and* $B/d0 \to \mu^+\mu^-$ *decays in* $p\bar{p}$ *collisions at* $\sqrt{s} = 1.9$ *6 TeV*, *Phys. Rev. Lett.* **93** (2004) 032001 [hep-ex/0403032].

[9] See DZero web page,
http://www-d0.fnal.gov/Run2Physics/WWW/results/prelim/B/B21/B21.pdf.

[10] CDMS collaboration, D.S. Akerib et al., *First results from the cryogenic dark matter search in the soudan underground lab*, *Phys. Rev. Lett.* **93** (2004) 211301 [astro-ph/0405033].

[11] K. Tobe and J.D. Wells, *Revisiting top-bottom-tau Yukawa unification in supersymmetric grand unified theories*, *Nucl. Phys.* **B 663** (2003) 123 [hep-ph/0301015].

[12] D. Auto et al., *Yukawa coupling unification in supersymmetric models*, *JHEP* **06** (2003) 023 [hep-ph/0302155].

[13] C. Balazs and R. Dermisek, *Yukawa coupling unification and non-universal gaugino mediation of supersymmetry breaking*, *JHEP* **06** (2003) 024 [hep-ph/0303161].

[14] R. Dermisek and S. Raby, *Bi-large neutrino mixing and CP-violation in an* SO(10) *SUSY GUT for fermion masses*, hep-ph/0507045.

[15] J.A. Bagger, J.L. Feng, N. Polonsky and R.-J. Zhang, *Superheavy supersymmetry from scalar mass a-parameter fixed points*, *Phys. Lett.* **B 473** (2000) 264 [hep-ph/9911255].

[16] F. Gabbiani, E. Gabrielli, A. Masiero and L. Silvestrini, *A complete analysis of FCNC and CP constraints in general SUSY extensions of the standard model*, *Nucl. Phys.* **B 477** (1996) 321 [hep-ph/9604387];
T. Besmer, C. Greub and T. Hurth, *Bounds on flavor violating parameters in supersymmetry*, *Nucl. Phys.* **B 609** (2001) 359 [hep-ph/0105292].

[17] K. Okumura and L. Roszkowski, *Weakened constraints from* $B \to s\gamma$ *on supersymmetry flavor mixing due to next-to-leading-order corrections*, *Phys. Rev. Lett.* **92** (2004) 161801; *Large beyond-leading-order effects in* $b \to s\gamma$ *in supersymmetry with general flavor mixing*, *JHEP* **10** (2003) 024 [hep-ph/0308102].

[18] J. Foster, K.-i. Okumura and L. Roszkowski, *New Higgs effects in B physics in supersymmetry with general flavour mixing*, *Phys. Lett.* **B 609** (2005) 102 [hep-ph/0410323]; *Probing the flavour structure of supersymmetry breaking with rare B-processes: a beyond leading order analysis*, hep-ph/0506146.

[19] C.K. Jung talk, http://nngroup.physics.sunysb.edu/uno/UNO04-Keystone/.

[20] R. Dermisek, A. Mafi and S. Raby, *SUSY GUTs under siege: proton decay*, *Phys. Rev.* **D 63** (2001) 035001 [hep-ph/0007213].

[21] T. Blazek, M. Carena, S. Raby and C.E.M. Wagner, *A global χ^2 analysis of electroweak data in* SO(10) *SUSY GUTs*, *Phys. Rev.* **D 56** (1997) 6919 [hep-ph/9611217].

[22] H.E. Haber and R. Hempfling, *The renormalization group improved Higgs sector of the minimal supersymmetric model*, *Phys. Rev.* **D 48** (1993) 4280 [hep-ph/9307201];
M. Carena, J.R. Espinosa, M. Quiros and C.E.M. Wagner, *Analytical expressions for radiatively corrected Higgs masses and couplings in the MSSM*, *Phys. Lett.* **B 355** (1995) 209 [hep-ph/9504316].

[23] M. Carena, M. Quiros and C.E.M. Wagner, *Effective potential methods and the Higgs mass spectrum in the MSSM*, *Nucl. Phys.* **B 461** (1996) 407 [hep-ph/9508343].

[24] D.E. Groom, et al., *The review of particle physics*, *Eur. Phys. J.* **C 15** (2000) 1.

[25] P. Langacker, talk at *Chicagoland seminar*, October 1999.

[26] M. Beneke and A. Signer, *The bottom $\bar{M}S$ quark mass from sum rules at next-to-next-to-leading order*, *Phys. Lett.* **B 471** (1999) 233 [hep-ph/9906475].

[27] T. Nihei, L. Roszkowski and R. Ruiz de Austri, *Towards an accurate calculation of the neutralino relic density*, *JHEP* **05** (2001) 063 [hep-ph/0102308]; *Exact cross sections for the neutralino wimp pair-annihilation*, *JHEP* **03** (2002) 031 [hep-ph/0202009].

[28] J. Edsjo and P. Gondolo, *Neutralino relic density including coannihilations*, *Phys. Rev.* **D 56** (1997) 1879 [hep-ph/9704361].

[29] T. Nihei, L. Roszkowski and R. Ruiz de Austri, *Exact cross sections for the neutralino slepton coannihilation*, *JHEP* **07** (2002) 024 [hep-ph/0206266].

[30] P. Gondolo, J. Edsjo, L. Bergstrom, P. Ullio and T. Baltz, http://www.physto.se/edsjo/darksusy/.

[31] R. Arnowitt, B. Dutta, T. Kamon and M. Tanaka, *Detection of $B_s \to \mu^+\mu^-$ at the Tevatron run II and constraints on the SUSY parameter space*, *Phys. Lett.* **B 538** (2002) 121 [hep-ph/0203069].

[32] P. Ball et al., *B decays at the LHC*, hep-ph/0003238.

[33] S. Baek, Y.G. Kim and P. Ko, *Neutralino dark matter scattering and $B_s \to \mu^+\mu^-$ in SUSY models*, *JHEP* **02** (2005) 067 [hep-ph/0406033].

[34] Y.G. Kim, T. Nihei, L. Roszkowski and R. Ruiz de Austri, *Upper and lower limits on neutralino WIMP mass and spin- independent scattering cross section and impact of new (g-2)(μ) measurement*, *JHEP* **12** (2002) 034 [hep-ph/0208069].

[35] G. Jungman, M. Kamionkowski and K. Griest, *Supersymmetric dark matter*, *Phys. Rept.* **267** (1996) 195 [hep-ph/9506380].

[36] IceCube collaboration, J. Ahrens et al., *The next generation neutrino telescope at the south pole*, *Nucl. Phys.* **118** *(Proc. Suppl.)* (2003) 388;
F. Halzen, *High-energy neutrino astronomy: from Amanda to IceCube*, astro-ph/0311004;
F. Halzen and D. Hooper, *Icecube-plus: an ultra-high energy neutrino telescope*, *JCAP* **01** (2004) 002 [astro-ph/0310152].

[37] J. Binney and S. Tremaine, *Galactic dynamics*, Princeton University Press, Princeton 1987.

[38] J.F. Navarro, C.S. Frenk and S.D.M. White, *The structure of cold dark matter halos*, *Astrophys. J.* **462** (1996) 563 [astro-ph/9508025]; *A universal density profile from hierarchical clustering*, *Astrophys. J.* **490** (1997) 493.

[39] B. Moore, S. Ghigna, F. Governato, G. Lake, T. Quinn, J. Stadel and P. Tozzi, *Dark matter substructure within galactic halos*, *Astrophys. J.* **524** (1999) 19.

[40] G. Bertone, P. Binetruy, Y. Mambrini and E. Nezri, *Annihilation radiation of dark matter in heterotic orbifold models*, hep-ph/0406083.

[41] D. Hooper and B.L. Dingus, *Limits on supersymmetric dark matter from EGRET observations of the galactic center region*, *Phys. Rev.* **D 70** (2004) 113007 [astro-ph/0210617].

[42] The HESS collaboration, F. Aharonian et al., *Very high energy gamma rays from the direction of sagittarius a**, astro-ph/0408145.

[43] L. Bergstrom, J. Edsjo and P. Ullio, *Cosmic antiprotons as a probe for supersymmetric dark matter?*, astro-ph/9902012.

[44] BESS collaboration, S. Orito et al., *Precision measurement of cosmic-ray antiproton spectrum*, *Phys. Rev. Lett.* **84** (2000) 1078 [astro-ph/9906426].

[45] J.L. Feng, K.T. Matchev and F. Wilczek, *Prospects for indirect detection of neutralino dark matter*, *Phys. Rev.* **D 63** (2001) 045024 [astro-ph/0008115].

[46] PAMELA collaboration, M. Pearce, *The status of the Pamela experiment*, *Nucl. Phys.* **113** *(Proc. Suppl.)* (2002) 314.

[47] AMS collaboration, J. Casaus, *The ams experiment: a magnetic spectrometer in space*, *Nucl. Phys.* **114** *(Proc. Suppl.)* (2003) 259.

[48] Muon g-2 collaboration, G.W. Bennett et al., *Measurement of the positive muon anomalous magnetic moment to 0.7 ppm*, *Phys. Rev. Lett.* **89** (2002) 101804 [hep-ex/0208001], erratum *ibid.* **89** (2002) 129903.

[49] M. Davier, S. Eidelman, A. Hocker and Z. Zhang, *Updated estimate of the muon magnetic moment using revised results from e^+e^- annihilation*, *Eur. Phys. J.* **C 31** (2003) 503 [hep-ph/0308213].

JHEP09(2005)029